



ATR activity controls stem cell quiescence via the cyclin F–SCF complex

Jayesh S. Salvi^{a,b}, Jengmin Kang^{a,b}, Soochi Kim^{a,b}, Alex J. Colville^{a,b}, Antoine de Morrée^{a,b,1}, Tine Borum Billeskov^{a,b,2}, Mikkel Christian Larsen^{a,b,3}, Abhijnya Kanugovi^{a,b}, Cindy T. J. van Velthoven^{a,b,4}, Karlene A. Cimprich^c, and Thomas A. Rando^{a,b,d,5,6}

Edited by Margaret Buckingham, Institut Pasteur, Paris, France; received August 26, 2021; accepted March 11, 2022

A key property of adult stem cells is their ability to persist in a quiescent state for prolonged periods of time. The quiescent state is thought to contribute to stem cell resilience by limiting accumulation of DNA replication–associated mutations. Moreover, cellular stress response factors are thought to play a role in maintaining quiescence and stem cell integrity. We utilized muscle stem cells (MuSCs) as a model of quiescent stem cells and find that the replication stress response protein, ATR (Ataxia Telangiectasia and Rad3-Related), is abundant and active in quiescent but not activated MuSCs. Concurrently, MuSCs display punctate RPA (replication protein A) and R-loop foci, both key triggers for ATR activation. To discern the role of ATR in MuSCs, we generated MuSC-specific ATR conditional knockout (ATR^{CKO}) mice. Surprisingly, ATR ablation results in increased MuSC quiescence exit. Phosphoproteomic analysis of ATR^{CKO} MuSCs reveals enrichment of phosphorylated cyclin F, a key component of the Skp1–Cul1–F-box protein (SCF) ubiquitin ligase complex and regulator of key cell-cycle transition factors, such as the E2F family of transcription factors. Knocking down cyclin F or inhibiting the SCF complex results in E2F1 accumulation and in MuSCs exiting quiescence, similar to ATR-deficient MuSCs. The loss of ATR could be counteracted by inhibiting casein kinase 2 (CK2), the kinase responsible for phosphorylating cyclin F. We propose a model in which MuSCs express cell-cycle progression factors but ATR, in coordination with the cyclin F–SCF complex, represses premature stem cell quiescence exit via ubiquitin–proteasome degradation of these factors.

muscle stem cells | quiescence | ATR | cyclin F | DNA:RNA hybrids

Many tissue-specific, adult stem cells persist in a reversible state of cell-cycle arrest, termed quiescence (1–4). Stem cell quiescence is regulated by multiple factors including p53, Rb, cyclin-dependent kinase inhibitors, such as p21 and p27, and Notch signaling (5–10). How these pathways may integrate to maintain stem cell quiescence remains unclear. Furthermore, it is unclear whether multiple pathways work in parallel to maintain quiescence or whether select factors are dynamically engaged in response to intrinsic and extrinsic cues.

Dysregulation or loss of quiescence often results in stem cell depletion and impaired tissue homeostasis (1, 11), suggesting that quiescence may protect cells from endogenous and exogenous insults to cell integrity. However, it is unclear how the properties of quiescent cells may confer high levels of resilience, allowing for long-term maintenance of stem cell pools. It has been proposed that the dormant state may protect stem cells from accumulating DNA replication–associated DNA damage, thereby ensuring their regenerative capacity in response to injury or other stimuli over the lifetime of an organism (11). Mice harboring engineered mutations in diverse DNA repair and response pathways display reduced functional potential of stem cells (12–15), highlighting the importance of genome-protective mechanisms in regenerative potential.

Intrinsic sources of DNA damage, such as reactive oxygen species, telomere erosion, DNA:RNA hybrids, and other non-B-form DNA, drive the need for efficient DNA repair (16, 17). These intrinsic sources of damage can enact stress response factors such as the replication stress response checkpoint kinase ATR (“Ataxia telangiectasia and Rad3 related”). Canonically, ATR responds to single-stranded DNA (ssDNA) structures coated by RPA (replication protein A) that are generated during DNA replication in the S phase of the cell cycle (18–20). ATR can also respond to RPA-coated ssDNA generated by DNA:RNA hybrids. Such a response is thought to occur at centromeres during mitosis to promote proper chromosome segregation, suggesting that ATR may have regulatory roles beyond DNA replication and the S phase of the cell cycle (21). ATR ablation in adult mice is reported to result in stem and progenitor cell loss, ultimately leading to defects in tissue homeostasis and the onset of aging-associated

Significance

The replication stress response protein, ATR, is active in quiescent muscle stem cells in response to DNA:RNA hybrids, and this activity maintains quiescence by ensuring degradation of key cell-cycle transition factors by the E3 ubiquitin ligase cyclin F–SCF complex. This is critical for understanding how stem cells regulate a state of prolonged and reversible cell-cycle arrest and how genome integrity is maintained over time. Together, these studies offer a unique picture of a molecular mechanism controlling stem cell quiescence.

Author affiliations: ^aPaul F. Glenn Center for the Biology of Aging, Stanford University School of Medicine, Stanford, CA 94305; ^bDepartment of Neurology and Neurological Sciences, Stanford University School of Medicine, Stanford, CA 94305; ^cDepartment of Chemical and Systems Biology, Stanford University School of Medicine, Stanford, CA 94305–5441; and ^dNeurology Service, VA Palo Alto Health Care System, Palo Alto, CA 94304

Author contributions: J.S.S. and T.A.R. designed research; J.S.S., J.K., S.K., A.J.C., A.d.M., T.B.B., M.C.L., A.K., and C.T.J.v.V. performed research; J.S.S., J.K., S.K., and C.T.J.v.V. analyzed data; J.S.S. and T.A.R. wrote the paper; and K.A.C. contributed expertise in ATR biology.

The authors declare no competing interest.

This article is a PNAS Direct Submission.

Copyright © 2022 the Author(s). Published by PNAS. This article is distributed under [Creative Commons Attribution-NonCommercial-NoDerivatives License 4.0 \(CC BY-NC-ND\)](https://creativecommons.org/licenses/by-nc-nd/4.0/).

¹Present address: Department of Biomedicine, Aarhus University, Aarhus 8000, Denmark.

²Present address: Department of Endocrinology and Internal Medicine, Steno Diabetes Center, Aarhus University, Aarhus 8000, Denmark.

³Present address: Department of Clinical Medicine, Comparative Medicine Lab, Aarhus University, Aarhus 8000, Denmark.

⁴Present address: Allen Institute for Brain Science, Seattle, WA 98109.

⁵Present address: Broad Stem Cell Research Center, University of California, Los Angeles, CA 90095.

⁶To whom correspondence may be addressed. Email: trando@mednet.ucla.edu.

This article contains supporting information online at <http://www.pnas.org/lookup/suppl/doi:10.1073/pnas.2115638119/-DCSupplemental>.

Published April 27, 2022.

phenotypes (22–24). These studies focused on tissues in which continuous cellular proliferation is required for organ maintenance, such as hair follicles and thymus, and did not explore the effects of depletion in quiescent stem cells (22–24). Thus, the question remains whether there is a role for ATR in quiescent stem cell maintenance.

In this paper, we demonstrate that muscle stem cells express ATR in the quiescent state, and ATR expression is down-regulated during stem cell activation. ATR expression in the quiescent cells corresponds to the presence of DNA:RNA hybrids, presumably triggering ATR to respond as a signal of DNA damage. Surprisingly, muscle stem cell-specific ATR ablation results in the loss of quiescence, demonstrating that ATR activity plays a role in the maintenance of the quiescent state. We discover a potential link between ATR and the SCF ubiquitin ligase complex in the maintenance of stem cell quiescence via suppression of SCF targets, such as E2F1, a key regulator of cell-cycle transitions. These studies suggest an ATR response to intrinsic sources of DNA damage in quiescent stem cells that maintains cellular quiescence by suppressing mechanisms of cell-cycle entry.

Results

We have previously characterized the *in vivo* transcriptome of MuSCs using mice that had been engineered to express uracil phosphoribosyltransferase (UPRT) specifically in MuSCs (25). When the mice are treated with 4-thiouracil (4tU), the 4tU is converted by UPRT into 4-thiouridine monophosphate which is then incorporated into newly transcribed RNA and allows labeling of RNA *in vivo* (26). We found that multiple DNA damage response factors were expressed in quiescent MuSCs (Fig. 1*A*). Intriguingly, we also observed that ATR was expressed in quiescent cells and was down-regulated as cells exited quiescence and entered the cell cycle (Fig. 1*A*). ATR is the master regulator of the replication stress response and responds directly to stalled replication forks and to DNA damage during the S phase of the cell cycle (27). Therefore, it was curious to find ATR expressed in a quiescent stem cell population. We confirmed the presence of ATR in quiescent MuSCs in muscle sections by measuring ATR fluorescence intensity in Pax7⁺ MuSCs (Fig. 1*B*). We observed greater ATR fluorescence intensity in Pax7⁺ cells relative to Pax7⁻ cells. We also found that ATR protein was expressed in freshly isolated MuSCs and, like the transcript, declined when these cells activated to enter the cell cycle (Fig. 1*C* and *SI Appendix, Fig. S1 A and B*). In contrast to ATR, ATM (“Ataxia telangiectasia mutated”), a gene whose protein product is a key mediator of DNA double-strand break responses, was not expressed in quiescent MuSCs but was markedly up-regulated upon activation (*SI Appendix, Fig. S1C*). Evidence that ATR is not only expressed but active in freshly isolated MuSCs was supported by analysis of the phosphorylation of a key downstream target of ATR, Chk1 (Checkpoint kinase-1). Phosphorylated Chk1 was detectable in quiescent MuSCs but was markedly less prevalent in MuSCs activated *in vivo* or *in vitro* (Fig. 1*D* and *SI Appendix, Fig. S1D*). These data suggest that ATR is expressed and active in quiescent MuSCs; however, it is unclear what stimuli may initiate ATR activity in the quiescent state.

ATR signaling is typically initiated by its recruitment to ssDNA via the ssDNA binding protein RPA (replication protein A) (18–20). In addition to recruiting ATR, RPA is phosphorylated by ATR (28). We observed RPA1 foci in quiescent MuSCs, and, as further evidence of ATR activity, we

also observed phosphorylated RPA2 (serine 33) foci (Fig. 2*A and B*). Because RPA foci formation is associated with persistent ssDNA, we sought evidence of structures that may contain ssDNA in quiescent MuSCs. Transcription coupled R-loops contain a DNA:RNA hybrid and ssDNA, which recruit RPA throughout the cell cycle (29). R-loops have been shown to stimulate ATR activation (21, 29–31). We stained for the hybrid component of R-loops in freshly isolated MuSCs and found evidence of hybrid foci (Fig. 2*C*). This staining was markedly reduced when the cells were pretreated with recombinant RNase H to degrade the RNA component and thus destabilize R-loops (Fig. 2*C*). To determine whether R-loop accumulation was transcription coupled, we treated MuSCs with the RNAPII inhibitor α -amanitin to disrupt messenger RNA transcription, the RNAPI inhibitor actinomycin-D to disrupt rRNA transcription, or the transcription elongation inhibitor DRB. The R-loop signal was significantly reduced upon treating with α -amanitin or DRB, but not actinomycin-D (Fig. 2*D*), suggesting that R-loop accumulation is dependent on RNAPII activity. We noted that hybrid foci colocalized with ATR and phospho-RPA foci (Fig. 2*E*), indicating that ATR may be recruited to R-loops and enact RPA phosphorylation.

We next sought to determine why R-loops accumulate in quiescent cells and whether a causal link existed between R-loops and ATR activation. RNaseH1 enzymatically degrades the RNA component of DNA:RNA hybrids, thereby ensuring genome integrity (32–34). We hypothesized that RNaseH1 levels may be lower in quiescent relative to activated MuSCs and thus may limit R-loop resolution. Indeed, Western blot and immunofluorescence analysis revealed a significant increase in RNaseH1 as MuSCs activated (Fig. 3*A and B*). This increase in RNaseH1 corresponded to a decline in hybrid fluorescence intensity during activation (Fig. 3*B*). These data suggest that RNaseH1 levels are below the threshold necessary to efficiently resolve R-loops in quiescent MuSCs, and, as the cells activate, they increase RNaseH1 production, which subsequently degrades DNA:RNA hybrids.

To explore whether disrupting R-loop resolution would affect ATR signaling, we knocked down RNaseH1 in MuSCs using a lentiviral construct expressing short hairpin RNA targeting RNaseH1 (shRNaseH1) or a scrambled nontargeting control. Confocal microscopy revealed a significant reduction in RNaseH1 mean fluorescence intensity upon transduction of shRNaseH1 relative to the nontargeting control (Fig. 3*C and D*). We observed an increase in hybrid fluorescence intensity upon RNaseH1 knockdown (Fig. 3*C and D*). Western blot analysis also revealed that levels of phosphorylated Chk1 and phosphorylated RPA2 were increased in shRNaseH1 transduced cells (Fig. 3*E and F*), suggesting that ATR activity increases in response to reduced RNaseH1 levels and increased R-loop accumulation.

R-loops are structurally and functionally associated with G-quadruplex DNA structures, which are formed from hydrogen bonding of guanine tetrads (35, 36). When G-quadruplex structures were stabilized by treatment of the cells with pyridostatin (PDS) (37), we observed an increase in both hybrid foci and RPA phosphorylation (*SI Appendix, Fig. S2 A–C*). RPA phosphorylation follows ATR recruitment (38, 39). Thus, we next asked whether PDS-induced RPA phosphorylation was dependent on ATR. The ATR-specific small-molecule inhibitor (i) VE821 (iATR) reduced phospho-RPA signal intensity, even in the presence of PDS (*SI Appendix, Fig. S2 B and C*), suggesting that stabilized G-quadruplex and R-loop-induced RPA phosphorylation was dependent on ATR. Furthermore, PDS

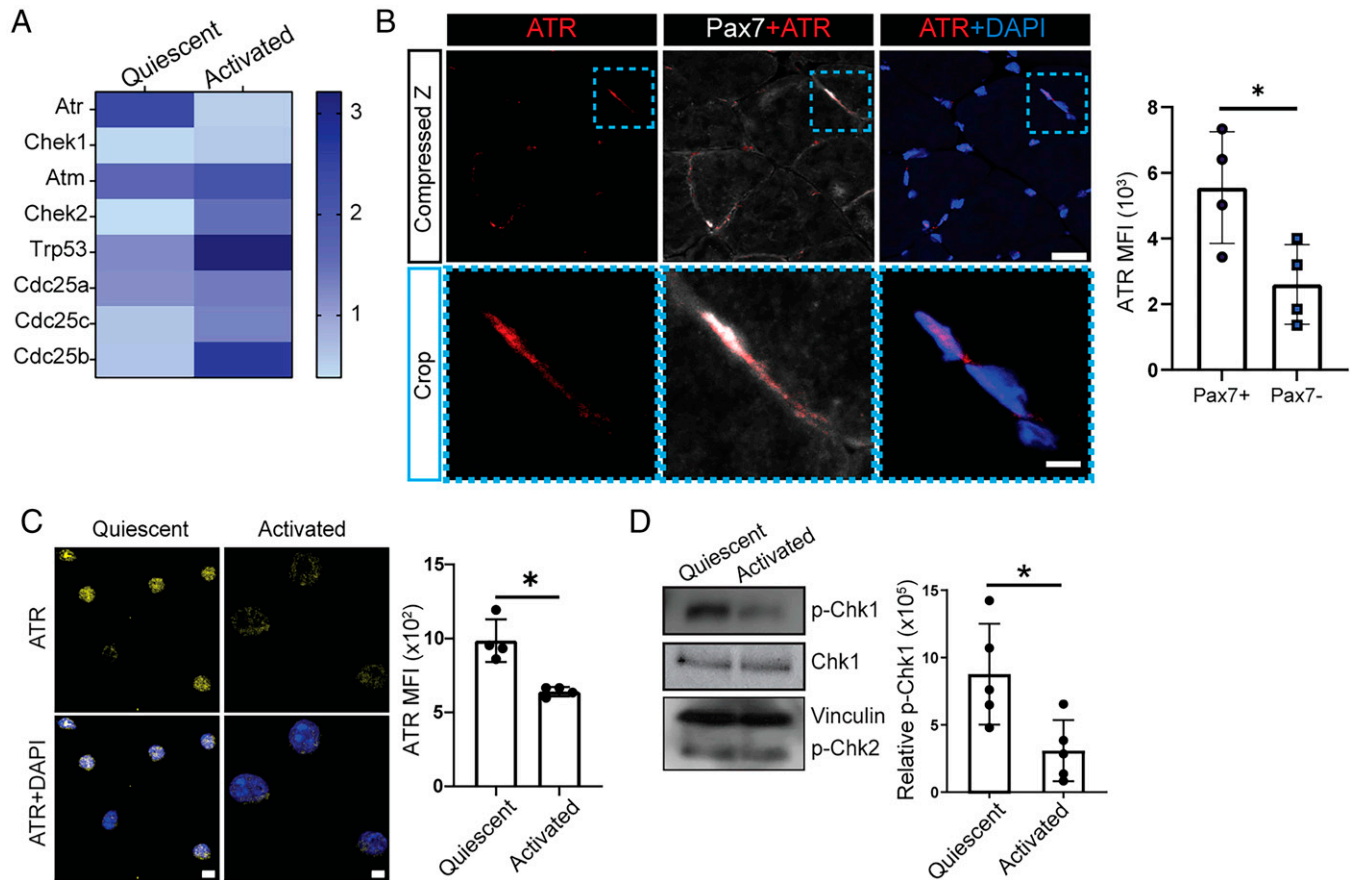


Fig. 1. ATR is expressed and active in quiescent MuSCs. (A) A heatmap depicting mean reads per million mapped reads (RPKM) values of select DNA damage response factors from nascent transcription sequencing in quiescent and activated MuSCs ($n = 4$ and $n = 3$ mice, respectively). (B) A representative compressed Z-stack confocal image of muscle section stained for ATR (red) and Pax7 (white) is shown (Top), with a cropped area (dotted blue box in Top) shown (Bottom). The quantification shows ATR mean fluorescence intensity (MFI) from Pax7-positive (Pax7+) and Pax7-negative (Pax7-) cells in muscle sections ($n = 4$; mean \pm SD; Student's t test with Welch's correction. (Scale bars, 10 μ m.) (C) A representative immunofluorescence image of quiescent and activated MuSCs stained for ATR is shown (Left). The quantification (Right) shows ATR MFI ($n = 4$; mean \pm SD; Student's t test with Welch's correction. (Scale bars, 5 μ m.) (D) Phosphorylated checkpoint kinase-1 (p-Chk1) was detectable at high levels in quiescent MuSCs but declined in MuSCs activated by in vivo muscle injury. A representative Western blot is shown (Left) and quantification (Right) of p-Chk1 relative to Chk1 and Vinculin ($n = 5$; mean \pm SD; Student's t test with Welch's correction). * $P < 0.05$.

treatment resulted in significant increase of phosphorylated Chk1 relative to control cells (SI Appendix, Fig. S2D). Together, these data suggest that stabilizing G-quadruplex structures and subsequently increasing R-loop levels results in ATR activation in quiescent MuSCs.

To explore whether degradation of R-loops would affect ATR signaling, we overexpressed RNaseH1 in MuSCs using a lentiviral construct. Confocal microscopy revealed a significant increase in RNaseH1 mean fluorescence intensity and a decrease in hybrid fluorescence intensity in cells transfected with the RNaseH1 lentivirus (Fig. 3 G and H). Western blot analysis revealed that levels of Chk1 and RPA2 phosphorylation were decreased in RNaseH1-overexpressing cells (Fig. 3 I and J), suggesting that ATR activity decreases in response to R-loop degradation. Together, these findings suggest that modulating R-loop levels alters ATR activity.

To explore the functional role of ATR in quiescent MuSCs, we generated mice in which ATR could be conditionally deleted specifically in this cellular population. We bred mice that have a tamoxifen-inducible Cre allele (CreER^{T2}) in the Pax7 locus with a strain in which the kinase domain of the ATR gene is flanked by loxP sites (40). The latter strain also has YFP knocked into the Rosa locus, allowing us to track MuSCs in which ATR is knocked out by YFP expression. Tamoxifen administration resulted in efficient knockout of

ATR in MuSCs in the ATR^{CKO} strain (Fig. 4A and SI Appendix, Fig. S3 A–C), and this was associated with reduced levels of phospho-Chk1 in those cells (Fig. 4B), confirming the loss of ATR activity.

Following deletion of ATR in MuSCs, we isolated YFP⁺ MuSCs and tested for any changes in quiescence and activation characteristics. Quiescent MuSCs are marked by the expression of Pax7, notch intracellular domain (NICD), and calcitonin receptor (CalcR) (10, 41–43). As MuSCs activate, they begin to express myoblast determination protein 1 (MyoD) (44, 45). We observed a significant decrease in the percentage of Pax7⁺ cells and an increase in the percentage of MyoD⁺ cells from ATR^{-/-} mice relative to those from ATR^{WT} mice (Fig. 4 C and D). Notch signaling is important for maintaining MuSC quiescence, and degradation of the NICD corresponds to a transition from G1 to S phase of the cell cycle (10, 46). ATR^{-/-} MuSCs displayed a significant reduction in the percentage of NICD⁺ cells relative to ATR^{WT} MuSCs (Fig. 4E). In contrast to Pax7 and NICD, CalcR was not significantly altered upon ATR ablation (SI Appendix, Fig. S3D), possibly due to CalcR not being lost until late activation (43). These data suggest that conditionally ablating ATR results in MuSCs displaying characteristics of activated cells.

We next examined muscles for any changes in quiescent MuSC phenotypes. We first injected ATR^{CKO} and ATR^{WT} mice

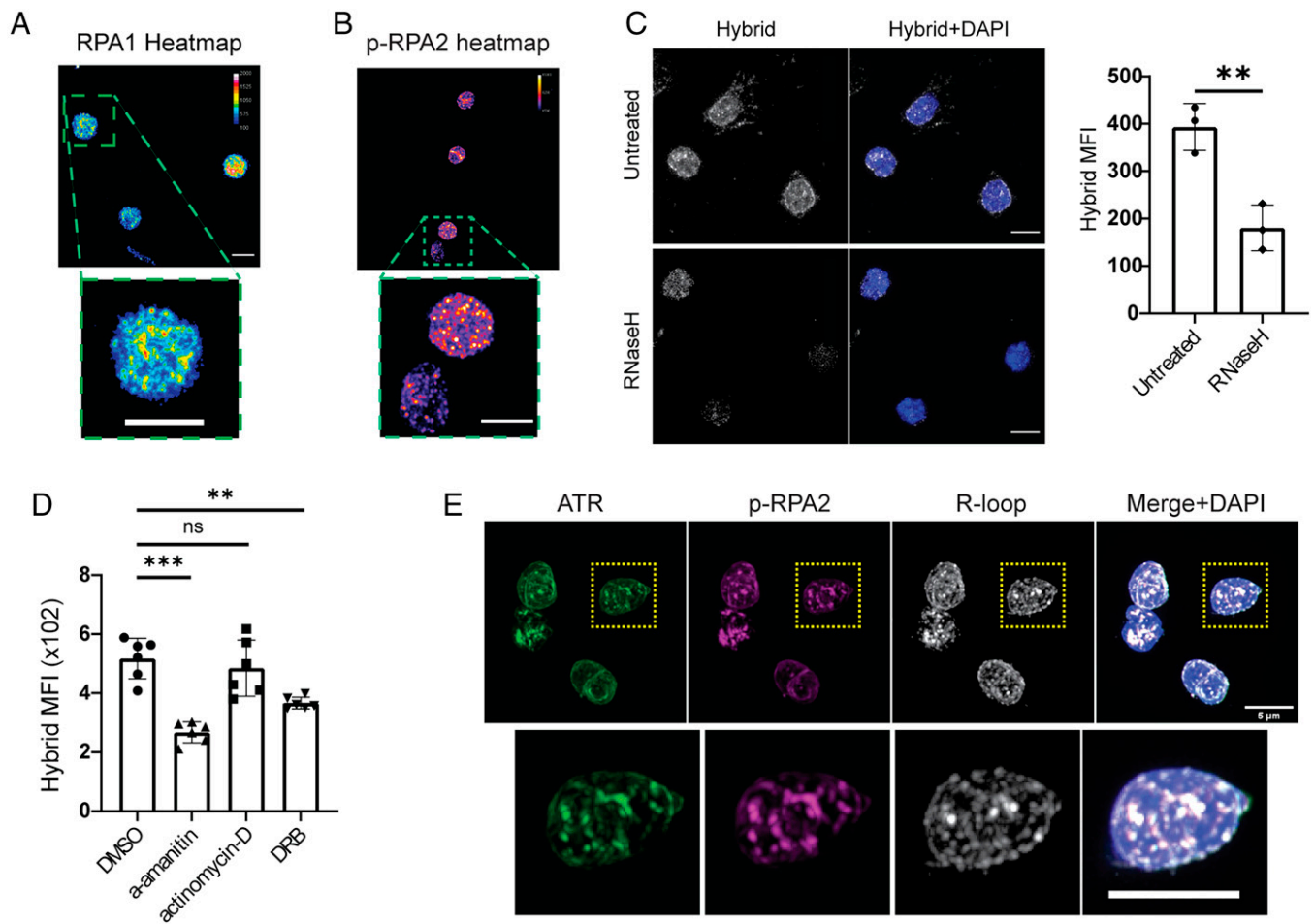


Fig. 2. R-loops can be detected in MuSCs. (A) A representative immunofluorescence image of quiescent MuSCs stained for RPA1 is shown (*Top*). The single cell in the dotted box is shown at higher magnification (*Bottom*). (B) A representative immunofluorescence image of quiescent MuSCs stained for phospho-RPA2 serine 33 (p-RPA2) is shown (*Top*). Cells in the dotted box are shown at higher magnification (*Bottom*). (C) A representative immunofluorescence image is shown (*Left*) and quantification of mean hybrid MFI from freshly isolated MuSCs, untreated or treated with recombinant RNase H ($n = 3$; mean \pm SD; Student's *t* test with Welch's correction). (D) Quantification of mean hybrid MFI from MuSCs treated with dimethyl sulfoxide (DMSO), a-amanitin, actinomycin-D, or DRB (5,6-dichloro-1-beta-ribo-furanosyl benzimidazole) for 4 h prior to fixation ($n \geq 4$; mean \pm SD; one-way ANOVA with multiple comparisons testing). (E) ATR and phospho-RPA2 colocalize with hybrid foci. A representative immunofluorescence image of quiescent MuSCs preextracted and stained for ATR, p-RPA2, and hybrids is shown (*Top*), with the cell in the dotted box shown at higher magnification (*Bottom*). ns = not significant, $**P < 0.01$, $***P < 0.001$. (Scale bars, 5 μ m).

intraperitoneally with the nucleotide analog 5-ethynyl-2'-deoxyuridine (EdU). Intriguingly, we observed a higher percentage of YFP⁺ EdU⁺ MuSCs in tibialis anterior (TA) muscle sections obtained from ATR^{eKO} mice and in freshly isolated ATR^{-/-} MuSCs extracted from bulk hindlimb muscles (Fig. 4 *F* and *G*), indicating that ATR^{-/-} MuSCs spontaneously exit quiescence in vivo. We also observed a higher percentage of Ki67⁺ MuSCs in ATR^{eKO} compared to ATR^{WT} mice (Fig. 4*H*), further confirming ATR^{-/-} MuSCs have an increased propensity to exit quiescence and enter the cell cycle. Indeed, MuSCs from ATR^{eKO} mice had an increase in RNA content by Pyronin-Y and RNaselect staining compared with those from ATR^{WT} mice (*SI Appendix, Fig. S3 E and F*), consistent with ATR^{-/-} MuSCs transitioning from a quiescent G0 state with low RNA content to a G1 state or other state in the cell cycle with higher RNA content (47).

We next asked whether pharmacological inhibition of ATR would also affect quiescence exit ex vivo. Once released from quiescence, the majority of MuSCs typically start incorporating EdU at ~36 h to 48 h in vitro, with small subsets of early activators incorporating EdU by 24 h (44). Consistent with our analysis of activation characteristics and in vivo findings, we noted a significant increase of EdU incorporation in cells

treated for 24 h with an ATR inhibitor in culture (*SI Appendix, Fig. S3 G*). We next wished to understand the relationship between increased or decreased R-loop levels and quiescence exit. We thus tested the effects of decreased or increased RNaseH1 expression as a way of modulating R-loop levels, on MuSCs maintained in quiescence ex vivo. RNaseH1 knockdown reduced EdU incorporation, and RNaseH1 overexpression resulted in increased EdU incorporation in MuSCs after 24 h of activation (*SI Appendix, Fig. S3 H and I*). These data further suggest that ATR may actively prevent quiescence exit, and that R-loops act as a barrier to quiescence exit.

A previous study had shown that ubiquitous deletion of ATR in adult mice resulted in depletion of proliferating progeny of stem cells in multiple tissues, but no phenotype was reported in quiescent stem cells (23, 24). Analysis of the number of Pax7⁺ cells 3 d to 5 d post tamoxifen revealed that deletion of ATR in MuSCs led to an increase in the Pax7⁺ cell numbers in TA muscles of ATR^{eKO} mice (*SI Appendix, Fig. S4 A and B*), consistent with our data that ATR^{-/-} MuSCs break quiescence and begin to proliferate. However, longer-term monitoring of Pax7⁺ cells in muscle section revealed a gradual decline of MuSCs in ATR^{eKO} mice relative to ATR^{WT} mice (*SI Appendix, Fig. S4 C*). Consistent with this

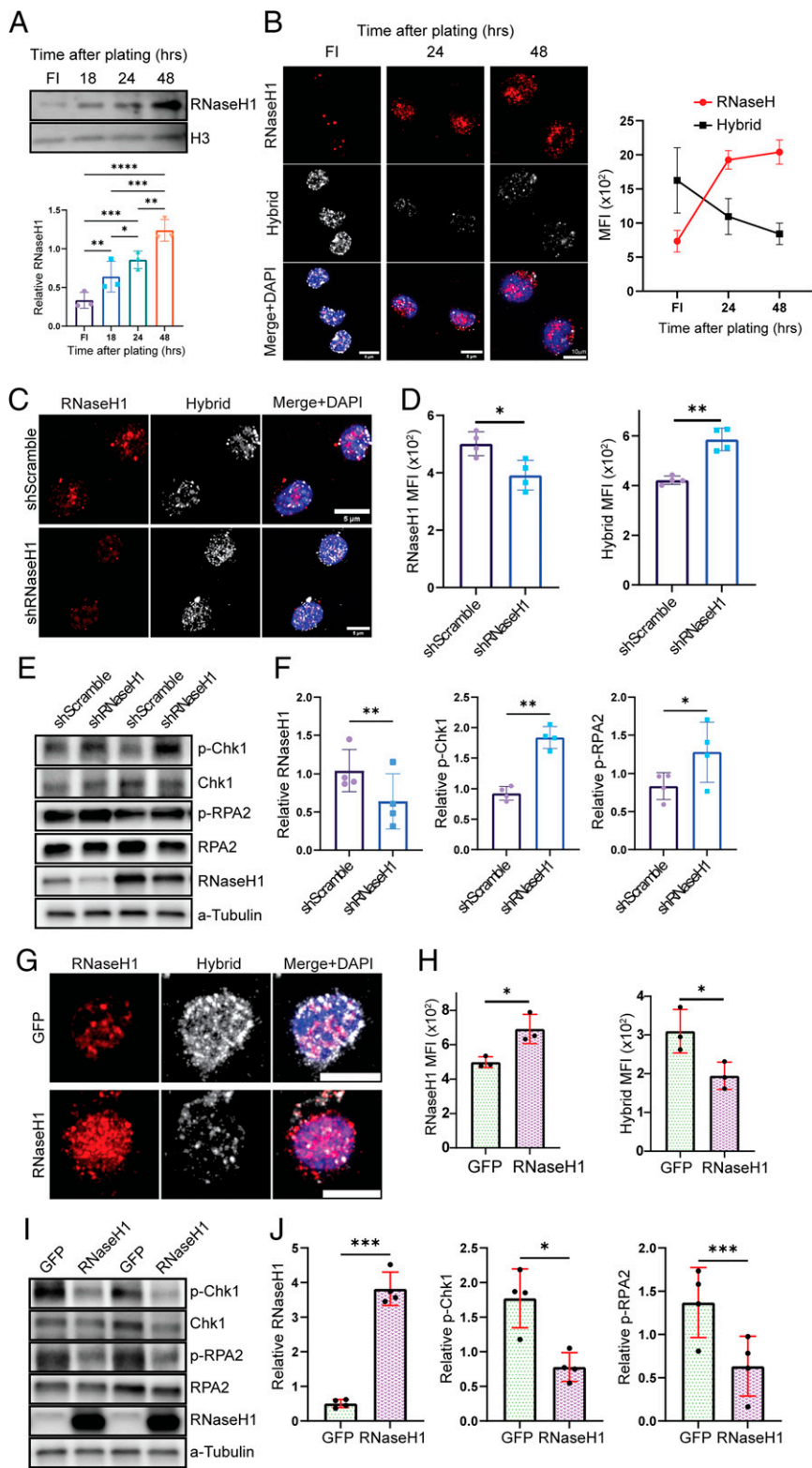


Fig. 3. Altering R-loop levels via RNaseH1 knockdown or overexpression results in concomitant ATR responses. (A) A representative Western blot is shown (Top) and quantification (Bottom) of RNaseH1 relative to H3 from FI MuSCs and from MuSCs activated for 18, 24, and 48 h ($n = 3$; mean \pm SD; one-way ANOVA with multiple comparisons testing). (B) Representative immunofluorescence images (Left) and MFI quantification (Right) of FI MuSCs and of MuSCs activated for 24 and 48 h and stained for RNaseH1 and hybrids. (Scale bars, 5 μ m.) (C) A representative immunofluorescence image of MuSCs transduced with either nontargeting shRNA (shScramble) or shRNA targeting RNaseH1 (shRNaseH1) and stained for RNaseH1 and hybrids. (Scale bars, 5 μ m.) (D) Quantification of mean RNaseH1 MFI (Left) and mean hybrid MFI (Right) ($n = 4$; mean \pm SD; Student's t test with Welch's correction). (E) Representative Western blot of MuSCs transduced with shScramble or shRNaseH1 and stained for RNaseH1, p-Chk1, Chk1, p-RPA2, RPA2, and α -tubulin. (F) Quantification of RNaseH1 relative α -tubulin (Left), p-Chk1 relative Chk1 (Middle), and p-RPA2 relative RPA2 (Right) from MuSCs transduced with shScramble or shRNaseH1 ($n = 4$; mean \pm SD; paired t test). (G) A representative immunofluorescence image of MuSCs transduced with either GFP or RNaseH1 and stained for RNaseH1 and hybrids. (Scale bars, 5 μ m.) (H) Quantification of mean RNaseH1 MFI and mean hybrid MFI ($n = 3$; mean \pm SD; Student's t test with Welch's correction). (I) Representative Western blot of MuSCs transduced with GFP or RNaseH1 and stained for RNaseH1, p-Chk1, Chk1, p-RPA2, RPA2, and α -tubulin. (J) Quantification of RNaseH1 relative α -tubulin (Left), p-Chk1 relative Chk1 (Middle), and p-RPA2 relative RPA2 (Right) from MuSCs transduced GFP or RNaseH1 ($n = 4$; mean \pm SD; paired t test); ns, not significant, * $P < 0.05$, ** $P < 0.01$, *** $P < 0.001$, **** $P < 0.0001$.

stem cell depletion upon ATR ablation, we noted increased terminal deoxynucleotidyltransferase-mediated dUTP nick end labeling positivity in freshly isolated ATR^{-/-} MuSCs (SI Appendix, Fig. S4D). However, we did not observe a significant increase in γ H2AX or ATM (SI Appendix, Fig. S4E and F), potentially suggesting that loss of ATR in quiescent MuSCs enacts apoptosis pathways unrelated to DNA double-strand breaks. We next injured TA muscles of ATR^{WT} and ATR^{CKO} mice and measured the cross-sectional area (CSA) of

regenerating muscle fibers. ATR^{CKO} mice exhibited impaired regeneration, indicated by increased frequency of smaller fibers and reduced mean CSA (SI Appendix, Fig. S4G and H). These findings indicate that ATR loss is detrimental to the long-term maintenance of quiescent stem cells and can hinder muscle regeneration after injury.

The exit from quiescence that we observed upon ATR ablation was unexpected. Therefore, we wished to understand the mechanism by which ATR maintains MuSCs in the quiescent state.

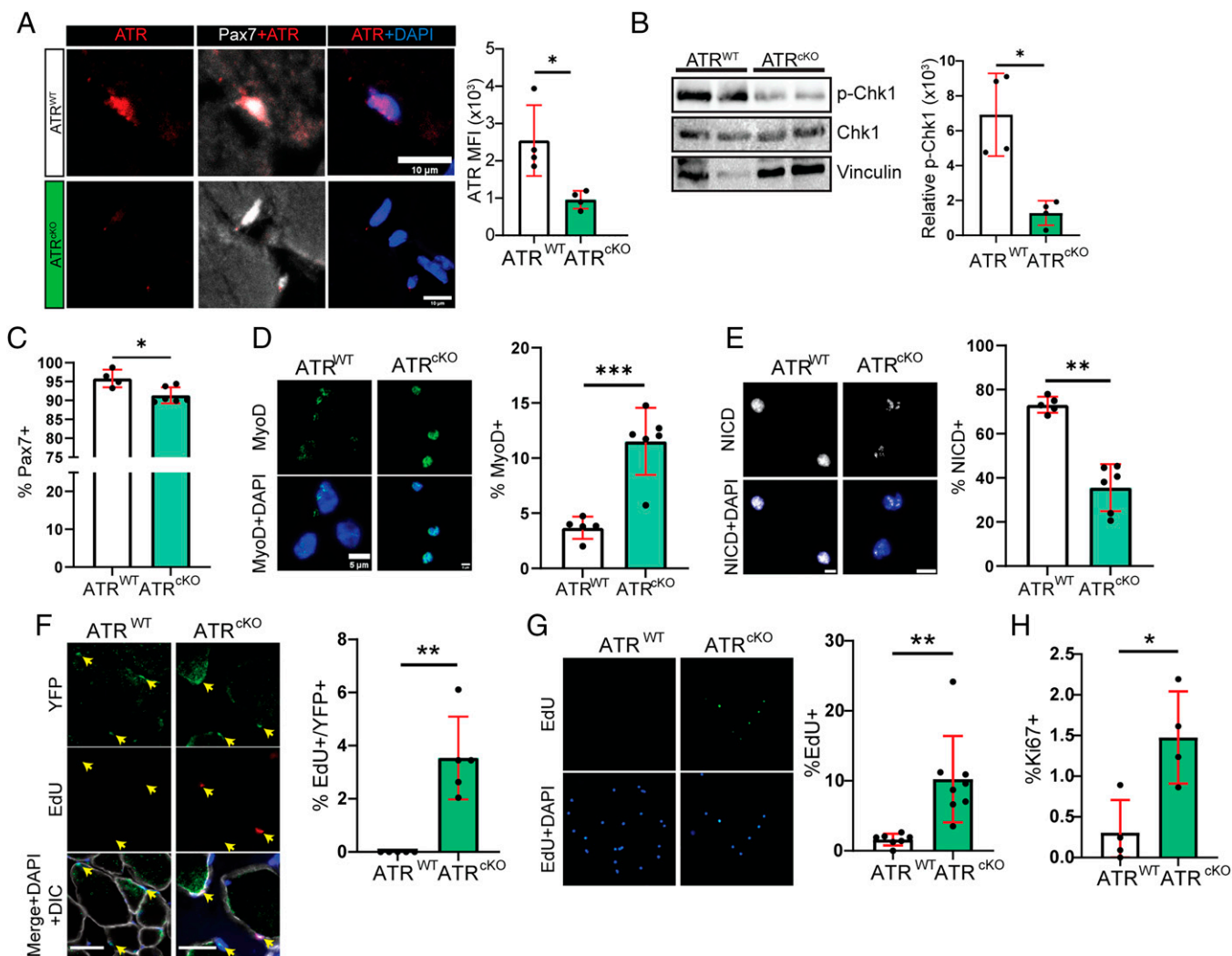


Fig. 4. ATR ablation in MuSCs results in quiescence exit. (A) Efficient knockout of ATR was detected by three-dimensional confocal microscopy in muscle sections. A representative compressed Z-stack confocal image of muscle section from ATR^{WT} and ATR^{CKO} mice stained for ATR (red) and Pax7 (white) is shown (Left) with quantification of ATR MFI in MuSCs (Right) ($n = 4$; mean \pm SD; Student's t test with Welch's correction). (Scale bars, 5 μ m.) (B) Diminished p-Chk1 in ATR^{CKO} MuSCs was observed as shown by the representative Western blot (Left) and quantification of multiple blots (Right) ($n = 4$; mean \pm SD; Student's t test with Welch's correction). (C) A decrease in the percentage of Pax7⁺ cells was observed in freshly isolated ATR^{CKO} MuSCs relative to ATR^{WT} MuSCs ($n \geq 4$; mean \pm SD; Student's t test with Welch's correction). (D) An increase in the percentage of MyoD⁺ cells was observed in freshly isolated ATR^{CKO} MuSCs relative to ATR^{WT} MuSCs. Representative images of MyoD⁺ cells are shown (Left) and quantification of percentage of MyoD⁺ MuSCs (Right) ($n \geq 5$; mean \pm SD; Student's t test with Welch's correction). (E) A decrease in percentage of NICD⁺ cells was observed in freshly isolated ATR^{CKO} MuSCs relative to ATR^{WT} MuSCs. Representative images of NICD⁺ cells are shown (Left) and quantification of percentage of NICD⁺ MuSCs (Right) ($n \geq 5$; mean \pm SD; Student's t test with Welch's correction) (Scale bars, 5 μ m.) (F) Increased percentage of EdU⁺/YFP⁺ MuSCs were observed in ATR^{CKO} mouse TA muscle sections. A representative muscle section from ATR^{WT} and ATR^{CKO} mouse is shown (Left) and quantification of EdU⁺/YFP⁺ MuSCs is on the Right ($n = 5$; mean \pm SD; Student's t test with Welch's correction). Yellow arrows indicate YFP⁺ MuSCs. (Scale bar, 25 μ m.) (G) An increase in percentage of EdU⁺ cells was observed in freshly isolated ATR^{CKO} MuSCs relative to ATR^{WT} MuSCs, from mice injected intraperitoneally once daily for 3 d with EdU. Representative images of EdU⁺ cells isolated from ATR^{WT} and ATR^{CKO} mouse are shown (Left) and quantification of EdU⁺ MuSCs (Right) ($n \geq 5$; mean \pm SD; Student's t test with Welch's correction). (H) An increase in percentage of Ki67⁺ freshly isolated MuSCs was observed in ATR^{CKO} mice relative to ATR^{WT} mice ($n = 4$; mean \pm SD; Student's t test with Welch's correction). * $P < 0.05$, ** $P < 0.01$, *** $P < 0.001$.

Canonically, ATR regulates cell-cycle progression through its kinase activity and the subsequent phosphorylation cascade that it enacts. Thus, we next sought to determine potential phosphorylation events downstream of ATR that may control quiescence in MuSCs. In order to obtain an unbiased assessment of the phosphoproteome regulated by ATR, we conducted a phosphoproteomic screen of MuSCs from ATR^{CKO} and ATR^{WT} mice to test for differential phosphoprotein profiles and potential downstream mediators of ATR. Proteins were subjected to phosphopeptide enrichment via column purification followed by liquid chromatography coupled to mass spectrometry. Of 727 enriched phosphopeptides, 276 (38%) were detected in both ATR^{CKO} and ATR^{WT} MuSCs, 146 (20%) were enriched in wild-type MuSCs, and 305 (42%) were enriched

in ATR^{-/-} cells (SI Appendix, Fig. S5A). To assess the significance of phosphopeptide changes between ATR^{CKO} and ATR^{WT} MuSCs and to normalize the averaged spectral intensities obtained from two separate phosphoproteomic experiments, we utilized a step-by-step regression analysis termed model-based analysis of proteomic data (MAP) (48). Using MAP normalization, phosphopeptide intensity scores were rescaled to fit the step-by-step regression-based model (SI Appendix, Fig. S5B). Utilizing MAP-normalized phosphopeptides, we established a phosphoproteome signature for ATR^{CKO} MuSCs.

Consistent with our findings that ATR^{CKO} MuSCs have an increased propensity to exit quiescence and enter the cell cycle, "cell division," "cell cycle," and "regulation of cell cycle" were

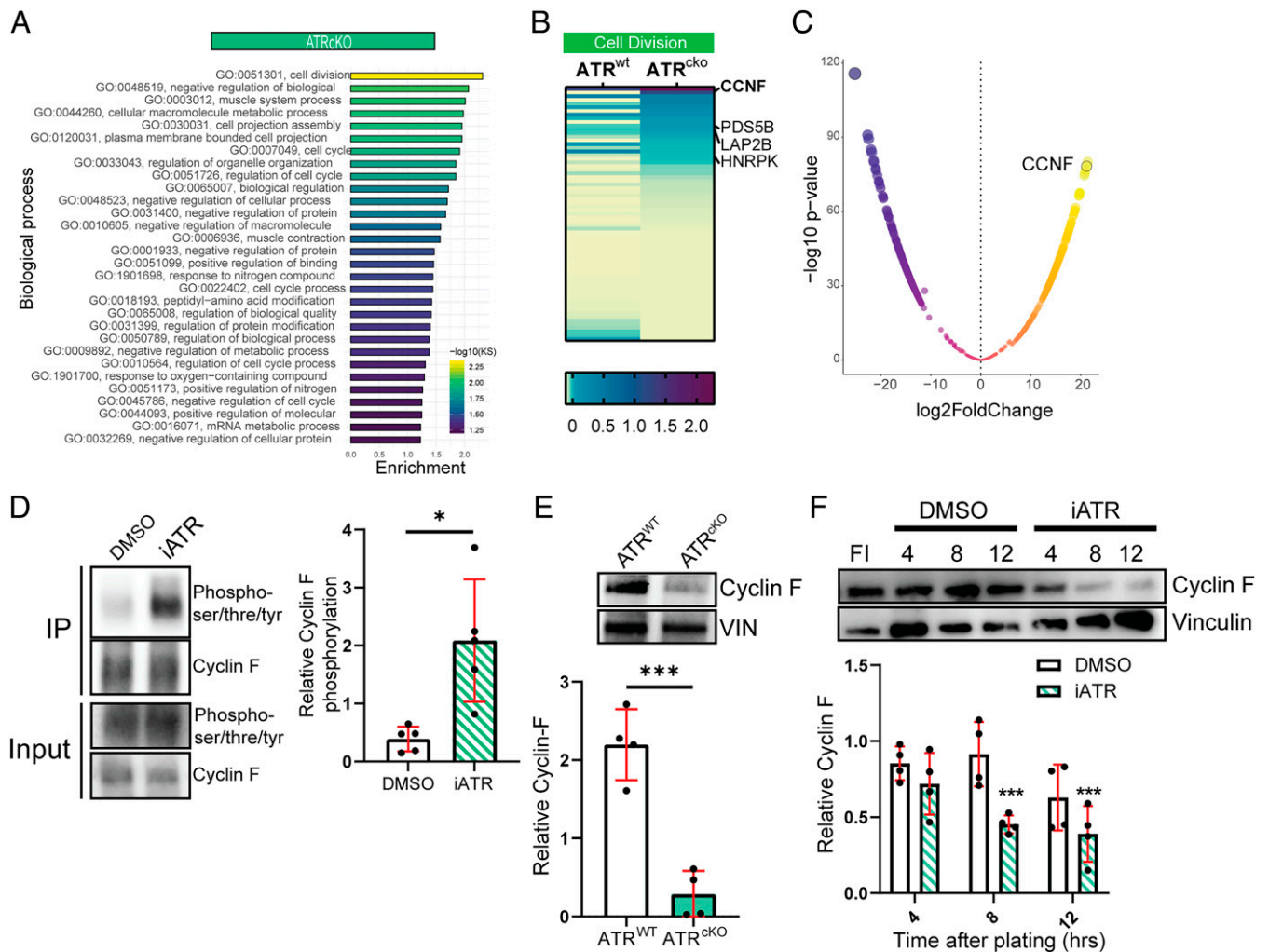


Fig. 5. Phosphoproteomic analysis of ATR^{WT} and ATR^{CKO} MuSCs identifies pathways associated with quiescence. (A) A bar plot representing GO term enrichment of the significantly up-regulated phosphopeptides following MAP normalization from ATR^{CKO} MuSCs. Colors and bar length represent $-\log_{10}$ of Kolmogorov-Smirnov value. (B) Top proteins from phosphoproteomic screen identified in GO term analysis as “Cell Division” are represented as a heatmap. CCNF (cyclin F) and other enriched proteins are highlighted. (C) Volcano plot of phosphopeptides following MAP normalization from ATR^{WT} and ATR^{CKO} MuSCs. Cyclin F is again highlighted as one of the most enriched phosphoproteins in ATR^{CKO} MuSCs. (D) Immunoprecipitation of cyclin F reveals the cyclin F phosphorylation state was altered upon loss of ATR activity. A representative Western blot is shown (Left) of immunoprecipitated (IP) or input samples, blotted for phosphoserine/phosphothreonine/phosphotyrosine and cyclin F from MuSCs treated with DMSO or iATR for 4 h. Quantification of phosphorylation relative cyclin F pulldown is shown (Right) ($n = 5$; mean \pm SD; Student’s t test with Welch’s correction). (E) Diminished cyclin F in ATR^{CKO} MuSCs was observed by Western blot, shown as a representative blot (Top) with quantification (Bottom) ($n = 4$; mean \pm SD; Student’s t test with Welch’s correction). (F) ATR inhibition results in rapid cyclin F degradation ex vivo. A Western blot of cyclin F in freshly isolated MuSCs, or in cells treated with DMSO or iATR for 4, 8, or 12 h, is shown (Top). Quantification of blots is shown (Bottom) ($n = 4$; mean \pm SD; two-way ANOVA with multiple comparisons testing; significance relative freshly isolated condition shown). DMSO and iATR treated samples were normalized to freshly isolated condition. * $P < 0.05$, *** $P < 0.001$.

found among the top gene ontology (GO) terms from analysis of phosphopeptides enriched in ATR^{CKO} cells (Fig. 5A). Shared within these GO terms and found as one of the most differentially enriched phosphoproteins in ATR^{CKO} MuSCs was the F-box and cyclin protein family member, cyclin F (CCNF) (Fig. 5B and C). To confirm whether cyclin F phosphorylation state was altered upon loss of ATR activity, we conducted cyclin F immunoprecipitation and monitored serine/threonine/tyrosine phosphorylation of cyclin F in cells treated with ATR inhibitor for 4 h, when cyclin F levels are most comparable between iATR and the control. In accordance with the idea that loss of ATR activity results in cyclin F phosphorylation, we observed increased phosphorylation in the ATR inhibitor-treated MuSCs (Fig. 5D). Phosphorylation of cyclin F may alter its function or target it for degradation (49–51). We found that cyclin F levels were markedly decreased in ATR^{CKO} MuSCs relative to ATR^{WT} MuSCs (Fig. 5E), suggesting that cyclin F is phosphorylated and subsequently degraded

upon ATR loss. To test whether cyclin F degradation was a feature of quiescence exit or unique to the loss of ATR activity, we monitored cyclin F levels over 12 h post isolation, with or without ATR inhibitor treatment. Control MuSCs did not display significant alterations to cyclin F over the 12-h time course (Fig. 5F). However, cyclin F levels declined after 18 h to 48 h in culture (SI Appendix, Fig. S5C), suggesting that cyclin F degradation may be a characteristic of later stages of MuSC activation. In contrast, we observed a progressive decline in cyclin F levels in the ATR inhibitor-treated MuSCs within 12 h post isolation (Fig. 5F). These data suggest that ATR actively maintains cyclin F abundance, and, upon ATR loss, cyclin F is phosphorylated and degraded.

Cyclin F acts as the substrate-binding domain for the Skp1–Cul1–F-box protein (SCF) ubiquitin ligase complex, and the cyclin F–SCF complex has been shown to directly regulate key factors involved in cell-cycle transitions, namely, the E2F

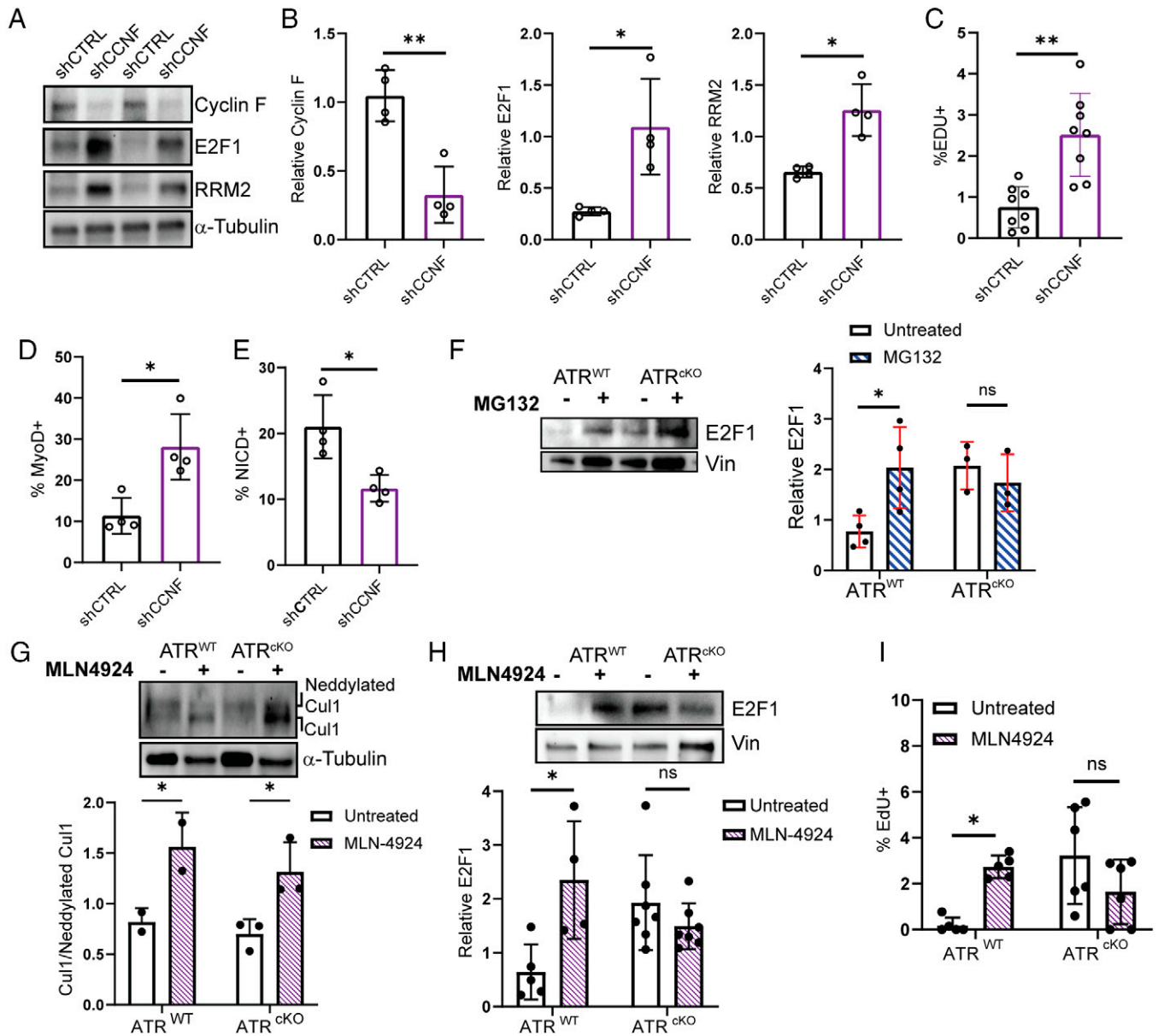


Fig. 6. ATR and the SCF complex promote E2F1 degradation to repress exit from the quiescent state. (A) A representative Western blot of MuSCs transduced with shCCNF or a scrambled nontargeting control (shCTRL) and blotted for cyclin F, E2F1, and RRM2. (B) Quantification of cyclin F (Left), E2F1 (Middle), and RRM2 (Right) from MuSCs transduced with shRNA targeting cyclin F shCCNF or shCTRL ($n = 4$; mean \pm SD; Student's t test with Welch's correction). (C) Cyclin F knockdown results in quiescence exit, similar to ATR^{cKO} MuSCs. Quantification of percentage of EdU⁺ MuSCs transduced with shCTRL or shCCNF and activated for 24 h ($n = 8$; mean \pm SD; Student's t test with Welch's correction). (D) An increase in percentage of MyoD⁺ cells was observed in MuSCs transduced with shCCNF relative to shCTRL-transduced MuSCs ($n = 4$; mean \pm SD; Student's t test with Welch's correction). (E) A decrease in percentage of NICD⁺ cells was observed in MuSCs transduced with shCCNF relative to shCTRL-transduced MuSCs ($n = 4$; mean \pm SD; Student's t test with Welch's correction). (F) Proteasome inhibition results in E2F1 accumulation in ATR^{WT} MuSCs, matching levels found in ATR^{cKO} MuSCs. A representative Western blot is shown (Top) and the quantification (Bottom) of E2F1 enrichment relative to Vinculin in ATR^{WT} and ATR^{cKO} MuSCs treated with either DMSO or proteasome inhibitor MG132 ($n \geq 3$; mean \pm SD; two-way ANOVA with multiple comparisons testing). (G) A representative Western blot (Top) and quantification (Bottom) of Cul1 (bottom band) relative to neddylated Cul1 (top band) enrichment in ATR^{WT} and ATR^{cKO} MuSCs treated with either DMSO or SCF complex inhibitor MLN-4924 ($n \geq 2$; mean \pm SD; two-way ANOVA with multiple comparisons testing). (H) SCF complex inhibition in ATR^{WT} MuSCs results in E2F1 accumulation matching levels found in ATR^{cKO} MuSCs. A representative Western blot is shown (Top) and quantification (Bottom) of E2F1 enrichment relative to Vinculin in ATR^{WT} and ATR^{cKO} MuSCs treated with either DMSO or SCF complex inhibitor MLN-4924 ($n \geq 3$; mean \pm SD; two-way ANOVA with multiple comparisons testing). (I) SCF complex inhibition in ATR^{WT} MuSCs results in quiescence exit similar to ATR^{cKO} MuSCs. Quantification of percentage of EdU⁺ MuSCs freshly isolated from ATR^{WT} and ATR^{cKO} mice treated with either DMSO or MLN-4924 ($n \geq 5$; mean \pm SD; two-way ANOVA with multiple comparisons testing). * $P < 0.05$, ** $P < 0.01$.

family of transcription factors and RRM2 ("ribonucleotide reductase M2") (50, 52–54). To first test whether cyclin F targets E2F1 or RRM2 for degradation, we knocked down cyclin F in MuSCs using a lentiviral construct expressing shRNA targeting cyclin F (shCCNF) or a scrambled nontargeting control (shCTRL). We observed efficient cyclin F knockdown in MuSCs transduced with shCCNF, and, concurrently, E2F1 and RRM2 levels increased significantly (Fig. 6 A and B).

Cyclin F knockdown also resulted in increased EdU incorporation, consistent with increased E2F1 and RRM2 driving cell-cycle entry (Fig. 6 C). Similar to $ATR^{-/-}$ MuSCs, cyclin F knockdown increased the percentage of MyoD⁺ and decreased the percentage of NICD⁺ cells, further indicating that cyclin F suppresses quiescent exit (Fig. 6 D and E).

Considering that E2F levels have been shown to fine-tune the depth of cellular quiescence (55), we focused on E2F1 in

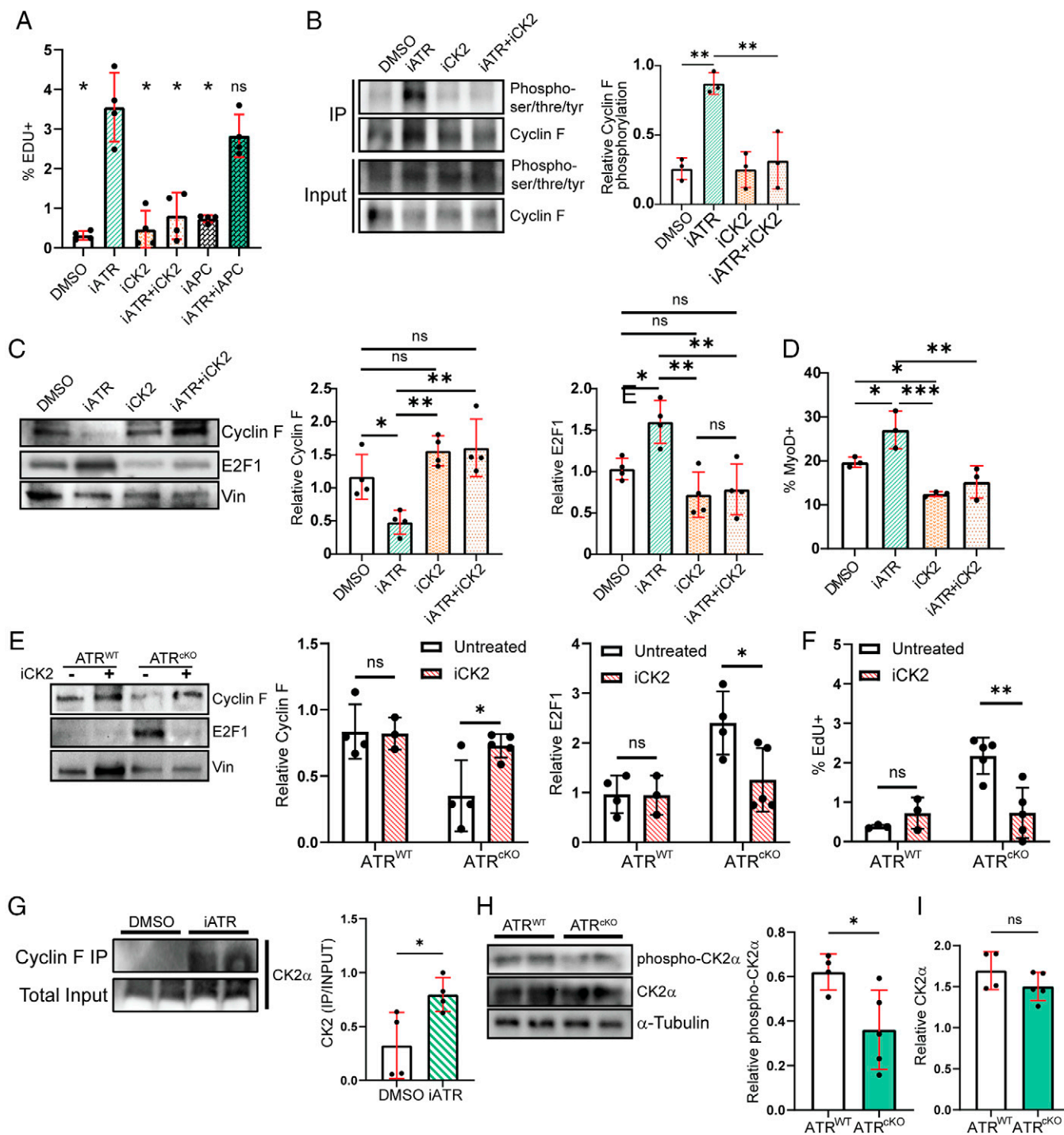


Fig. 7. Inhibiting CK2 restores cyclin F activity and represses exit from the quiescent state in ATR ablated MuSCs. (A) Exit from quiescence in ATR-inhibited MuSCs was repressed by CK2 inhibition but not APC inhibition. Quantification of percentage of EdU⁺ MuSCs treated with DMSO, iATR (5 μ M), CK2 inhibitor CX4945 (iCK2; 5 μ M), iATR+iCK2, APC inhibitor TAME (iAPC; 5 μ M), or iATR+iAPC ($n \geq 4$; mean \pm SD; one-way ANOVA with multiple comparisons testing; significance relative iATR condition shown). (B) Immunoprecipitation of cyclin F revealed that cyclin F phosphorylation upon ATR inhibition was decreased by CK2 inhibition. A representative Western blot is shown (Left) of IP or input samples, blotted for phosphoserine/phosphothreonine/phosphotyrosine and cyclin F from MuSCs treated with DMSO, iATR (5 μ M), CK2 inhibitor CX4945 (iCK2; 5 μ M), or iATR+iCK2, for 4 h. Quantification of phosphorylation relative cyclin F pull-down is shown (Right) ($n = 3$; mean \pm SD; Student's *t* test with Welch's correction). (C) Representative Western blot and quantifications of cyclin F and E2F1 in MuSCs treated with DMSO, iATR (5 μ M), or iCK2 (5 μ M) for 24 h ($n = 4$; mean \pm SD; one-way ANOVA with multiple comparisons testing). (D) Quantification of the percentage of MyoD⁺ cells from MuSCs treated with DMSO, iATR (5 μ M), CK2 inhibitor CX4945 (iCK2; 5 μ M), or iATR+iCK2, for 24 h ($n = 3$; mean \pm SD; one-way ANOVA with multiple comparisons testing). (E) Representative Western blot and quantifications of cyclin F and E2F1 enrichment in ATR^{WT} and ATR^{cKO} MuSCs treated with either DMSO or iCK2 *in vivo* ($n \geq 3$; mean \pm SD; two-way ANOVA with multiple comparisons testing). (F) Quantification of percentage of EdU⁺ MuSCs freshly isolated from ATR^{WT} and ATR^{cKO} mice treated with either DMSO or iCK2 ($n \geq 3$; mean \pm SD; two-way ANOVA with multiple comparisons testing). (G) Immunoprecipitation of cyclin F reveals CK2 binding was altered upon loss of ATR activity. A representative Western blot is shown (Left) of IP or input samples, blotted for CK2 from MuSCs treated with DMSO or iATR for 4 h. Quantification of CK2 IP relative to Input is shown (Right) ($n = 4$; mean \pm SD; Student's *t* test with Welch's correction). (H) A representative Western blot stained for phospho-CK2 α , CK2 α , and α -tubulin is shown (Left) and quantification of phospho-CK2 α enrichment relative to CK2 α from ATR^{WT} and ATR^{cKO} MuSCs is shown (Right) ($n = 4$; mean \pm SD; Student's *t* test with Welch's correction). (I) Quantification of CK2 α enrichment relative to α -tubulin from ATR^{WT} and ATR^{cKO} MuSCs ($n = 4$; mean \pm SD; Student's *t* test with Welch's correction). * $P < 0.05$, ** $P < 0.01$, *** $P < 0.001$.

subsequent experiments. If E2F1 abundance in quiescent MuSCs is controlled by its ubiquitination and subsequent proteasomal degradation, we expected that inhibiting the proteasome would result in E2F1 accumulation. Indeed, *ex vivo* treatment of wild-type MuSCs with the proteasome inhibitor, MG132, resulted in significant accumulation of E2F1 (Fig. 6*F*). Proteasome inhibition did not further increase E2F1 levels in ATR^{-/-} MuSCs (Fig. 6*F*). These data suggest that E2F1 protein in MuSCs is degraded by the proteasome in an ATR-dependent manner.

To test, *in vivo*, whether the cyclin F–SCF complex is responsible for targeting E2F1 for degradation, we treated ATR^{CKO} and ATR^{WT} mice with the neddylation inhibitor MLN-4924, which inhibits the cullin RING ligase (CRL) subunit of the SCF complex. Treatment with MLN-4924 significantly reduced Cul1 neddylation relative to vehicle-treated controls (Fig. 6*G*), indicating efficient *in vivo* inhibition of the CRL complex. Similar to *ex vivo* proteasome inhibition, *in vivo* CRL inhibition resulted in a significant increase of E2F1 levels in ATR^{WT} MuSCs but not in ATR^{CKO} MuSCs (Fig. 6*H*). Consistent with increased E2F1 levels, *in vivo* CRL inhibition increased the percentage of EdU⁺ MuSCs from ATR^{WT} mice relative to untreated ATR^{WT} mice (Fig. 6*I*). In contrast, CRL inhibition in ATR^{CKO} mice did not result in a significant difference in EdU incorporation relative to untreated ATR^{CKO} mice (Fig. 6*J*). Taken together, these data indicate that inhibiting the cyclin F–SCF complex in ATR^{WT} mice can phenocopy ATR^{-/-} MuSCs in terms of E2F1 levels and propensity to enter the cell cycle.

Based on these findings, we predicted that restoring cyclin F levels and SCF complex activity would rescue the loss of quiescence phenotype of ATR^{-/-} MuSCs by reducing E2F1 levels. Casein kinase II (CK2) dependent phosphorylation as well as anaphase promoting complex (APC) dependent ubiquitination and degradation can control cyclin F protein levels (51, 56). CK2 phosphorylation of cyclin F can also mediate the ubiquitin ligase activity of the SCF complex (50). To first investigate whether either CK2 or APC lie downstream of ATR in promoting MuSC quiescence, we measured EdU incorporation of MuSCs treated *ex vivo* with the CK2-specific inhibitor, CX-4945, or the APC-specific inhibitor, TAME, in addition to ATR inhibition. We found that CK2 inhibition, but not APC inhibition, significantly reduced quiescence exit relative to MuSCs treated with the ATR inhibitor alone (Fig. 7*A*). Furthermore, CK2 inhibition restored cyclin F phosphorylation, and cyclin F and E2F1 protein abundance to wild-type levels even in the presence of the ATR inhibitor (Fig. 7*B* and *C*). Inhibiting CK2 also significantly reduced the percentage of MyoD⁺ MuSCs treated with the ATR inhibitor (Fig. 7*D*). These data suggest that inhibiting CK2 *in vitro* can rescue many of the phenotypes associated with ATR loss in MuSCs.

To determine whether inhibiting CK2 would impact cyclin F levels, E2F1 accumulation, and MuSC quiescence in ATR^{CKO} mice, we treated ATR^{CKO} and ATR^{WT} mice with CX-4945 to inhibit CK2. In ATR^{WT} mice, in which, presumably, CK2 activity is low, cyclin F–SCF activity is high, and E2F1 levels are low, further inhibiting CK2 activity with the CK2 inhibitor did not further reduce E2F1 levels or affect MuSC quiescence (Fig. 7*E* and *F*). By contrast, treatment of ATR^{CKO} mice with CX-4945 led to a restoration of cyclin F levels, a reduction of E2F1 levels, and a maintenance of quiescence (Fig. 7*E* and *F*).

To determine how ATR might control cyclin F levels via CK2, we first asked whether ATR inhibition altered CK2 binding to cyclin F and found that ATR inhibition increased CK2 α enriched in the cyclin F immunoprecipitate (Fig. 7*G*). We then asked whether ATR inhibition might impact CK2 phosphorylation,

since CK2 α posttranslational modifications can modulate its substrate selectivity (57, 58). Indeed, there was a significant reduction in CK2 α phosphorylation upon ATR ablation and MuSC activation (Fig. 7*H* and *SI Appendix*, Fig. S6*A*). We next asked whether ATR controlled CK2 protein abundance or overall activity in any way. We did not observe any change to CK2 α levels in either ATR^{CKO} MuSCs or activating MuSCs (Fig. 7*I* and *SI Appendix*, Fig. S6*A*). Our phosphoproteomic analysis did enrich unique peptides for potential CK2 targets other than cyclin F, but we did not observe any bias in terms of the number of peptides enriched toward either ATR^{WT} or ATR^{CKO} (*SI Appendix*, Fig. S6*B*). Furthermore, ATR knockout did not significantly alter phosphorylation of key CK2 substrates, β -catenin and AKT (*SI Appendix*, Fig. S6*E*). To test for CK2 activity more generally, we measured the abundance of proteins containing the CK2 phosphorylation consensus sequence (pS/pTDXE motif). We noted a significant reduction in the pS/pTDXE motif-containing proteins upon CK2 inhibition with CX-4945 (*SI Appendix*, Fig. S6*C*). However, we did not observe any change in abundance of phosphorylated putative CK2 target proteins in either ATR^{-/-} or ATR inhibitor-treated MuSCs (*SI Appendix*, Fig. S6*C* and *D*). These data support the hypothesis that ATR maintains MuSC quiescence by a regulatory cascade that suppresses cyclin F–SCF targets in MuSCs (*SI Appendix*, Fig. S6*F*). In the absence of ATR, CK2 α phosphorylation is decreased, increasing its binding to cyclin F without altering the overall activity of CK2, increasing cyclin F phosphorylation, and targeting cyclin F for degradation. Consequently, cyclin F–SCF activity is reduced, leading to an increase in E2F1 levels and markers of activation such as MyoD, and an increased propensity of MuSCs to exit the quiescent state and enter the cell cycle (*SI Appendix*, Fig. S6*F*).

Discussion

In this study, we have discovered an unexpected role of ATR in maintaining quiescence of a stem cell population. This appears to be independent of the role of ATR in mediating the response to replicative stress, but the expression and activation of ATR are associated with the accumulation of R-loops in quiescent MuSCs. Intriguingly, when ATR is ablated in quiescent MuSCs, the cells spontaneously exit the quiescent state and enter the cell cycle. This transition appears to be due to the inhibition of the cyclin F–SCF ubiquitin ligase complex in ATR^{-/-} MuSCs, leading to a stabilization of cyclin F–SCF target proteins, such as E2F1, and thus promoting cell-cycle entry. These findings suggest that ATR activity is a regulator of quiescence by suppressing cyclin F–SCF targets via this regulatory cascade.

MuSC quiescence is actively maintained by multiple pathways. The first demonstration of active regulation of quiescence was the finding that deletion of the transcriptional regulator of the Notch signaling pathway, RBP-J, led to spontaneous activation of quiescent MuSCs (10). This has subsequently been shown to be due, at least in part, to the regulation of the *Col5a1* gene by the Notch pathway (59). Another regulator that was found to promote MuSC quiescence is the microRNA, miR-489 (60). This microRNA was found to promote quiescence by suppressing the expression of the protooncogene, *Dek*. When miR-489 was inhibited, *Dek* expression increased and promoted the proliferation of myogenic progenitors. Another microRNA, miR-708, was subsequently also found to regulate MuSC quiescence by targeting the transcript of the focal adhesion protein, Tensin3 (61). Clearly, multiple parallel pathways integrate to promote MuSC quiescence. The findings of the role of ATR in promoting quiescence appear to work in parallel

to those already described, but there may be cross-talk at the level of expression of genes related to cell-cycle entry.

Consistent with previous studies in proliferating cells (62–64), DNA:RNA hybrid accumulation in quiescent MuSCs is dependent on RNAPII activity. However, the question of why persistent R-loops form in lowly transcribing cells such as quiescent MuSCs remains unclear. Generally, R-loop accumulation is linked to high transcription rates; however, high RNA levels do not ensure R-loop formation, and others have shown that accumulation of RNA in the nucleus is not sufficient to cause R-loop accumulation (65–67). R-loops are regulated by multiple factors at the level of formation and resolution (68). The most notable of these are the RNaseH enzymes which degrade the RNA component of DNA:RNA hybrids (32–34). Quiescent MuSCs express low levels of RNaseH1 which is up-regulated during activation (25). Thus R-loops may escape degradation and result in ATR activation in quiescent MuSCs. Our work indicates that stabilization of R-loops during quiescence leads to increased ATR activity and perturbed cell-cycle entry. We propose that ATR activity preserves the quiescent state until sufficient RNaseH1 is expressed, R-loops are resolved, and the cell can properly transition to the next phase of the cell cycle. In this regard, a recent study in yeast is relevant in showing that RNaseH1 responds to R-loops throughout the cell cycle (69), although this study did not explore RNaseH1 expression in cells that were in a quiescent state. At present, we do not have data to explain, mechanistically, how RNaseH1 expression remains low in quiescent MuSCs or is increased during the activation process. Clearly, studies that reveal how steady-state levels of RNaseH1 transcript and protein are regulated in quiescent and activating MuSCs, or in other quiescent cells, will be of great interest.

Whereas ATR is studied primarily in terms of the response to replicative stress in the S phase (70), R-loop-responsive roles of ATR have also been reported. For example, ATR promotes faithful chromosome segregation during mitosis by detecting R-loops, coordinates with RNA helicases to prevent aberrant hybrid accumulation and replication–transcription collisions, and protects against R-loop induced double-strand breaks (21, 31, 71). ATR also guides other cell-cycle phase transitions. A recent study revealed a role for ATR in enforcing an S-to-G2 checkpoint (72). During S phase, ATR prevents the accumulation of mitosis factors. When ATR is inhibited, cells prematurely enter mitosis, resulting in underreplicated DNA and DNA damage. In order to ensure a proper S-to-G2 transition, ATR suppresses the phosphorylation and activity of the mitotic transactivator, FoxM1 (72). In this regard, our work also establishes ATR as a suppressor of premature cell-cycle transitions, although, in our case, it is a G0-to-G1 transition. In addition, we also establish a noncanonical signaling role for ATR in this suppressive capacity that links regulation of cyclin F via CK2 to quiescence maintenance. There also may be some interplay between ATR, FoxM1, and the SCF complex in that FoxM1 binds to promoters of the Skp2 and Cks1 subunits of the SCF complex and is required for their expression (73). Through the SCF complex, FoxM1 inhibits p21 and p27 expression and thereby controls the G1/S transition (73, 74). Intriguingly, others have linked FoxM1 to quiescence regulation in hematopoietic stem cells (75), although it is unexplored whether the SCF complex is involved in this pathway.

Germline inactivation of ATR is embryonic lethal (76, 77), and ATR ablation during neural development results in the

specific loss of neural progenitors (78). In adult animals, ATR depletion results in premature aging phenotypes driven by a loss of progenitor cells in tissues where active cycling is required for maintenance (23, 24). Our work expands on the role of ATR in proliferating cells into the unexpected realm of quiescent stem cells, and we propose that this quiescent-specific role for ATR protects stem cells from premature activation, which may leave the cells vulnerable to intrinsic drivers of DNA damage, such as R-loops. E2F1 levels have been proposed as a rheostat for cell expansion or cell death (79). Upon DNA damage induction, E2F1 cooperates with p53 to promote antiapoptotic signaling pathways (80), and E2F1 overexpression leads to apoptosis (81). Recent work has also linked the SCF complex to E2F regulation and cell fate decisions (54). Thus, by coordinating with the SCF complex and modulating E2F1 levels, ATR may prove to be a guardian of quiescent stem cells.

Methods

MuSC Isolation. For MuSC isolation, we followed the previously described protocol (82), with the following modifications: Hind-limb muscles were separately digested with collagenase II for 1 h in 10 mL of medium (Ham's F-10 [HyClone] supplemented with 10% horse serum and 1% penicillin/streptomycin). Tissues were washed with fresh medium, spun down at $500 \times g$ for 5 min, taken up in 10 mL of medium with collagenase II and dispase, and incubated for 30 min. Mononucleated cells were stained for 1 h with anti-CD31 (MEC 13.3, BD Bioscience), anti-CD45 (30-F11, BD Bioscience), anti-VCAM (429, BD Bioscience), and muscle regeneration anti-Sca-1 antibodies (D7; Biolegend) (all at 1:75) and sorted using a BD Fluorescent Activated Cell Sorting (BD-FACS Aria II and III). Purity was confirmed by resort or by Pax7 immunofluorescence stain. MuSCs from Pax7^{CreER/+}; Rosa^{eYFP/+} mice were purified by gating mononuclear eYFP-positive cells using a BD-FACS Aria II or BD-FACS Aria III. Flow cytometry and/or FACS was done with instruments in the Palo Alto Veterans Institute for Research (PAVIR) FACS Core, which is supported by the US Department of Veterans Affairs (VA), PAVIR, and NIH.

EdU Incorporation Assay. To assess the percentage of MuSCs exiting quiescence in culture, FACS-isolated MuSCs were plated with 5 μ M EdU (Thermo Fisher). After 24 h, cells were fixed and stained with the Click-iT EdU Imaging Kit (Thermo Fisher) and DAPI. Percentage EdU⁺ was calculated as the number of EdU⁺ over total DAPI⁺ cells. To assess EdU incorporation in vivo, mice were injected intraperitoneally with 10 mg/mL EdU in phosphate-buffered saline. Mice were injected once daily for three subsequent days with 100 μ L of EdU solution.

Extended materials and methods are provided within *SI Appendix*.

Data and Materials Availability. The mass spectrometry proteomics data have been deposited to the ProteomeXchange Consortium via the publicly accessible Proteomics Identifications Database (PRIDE) partner repository with the accession number [PXD028432](https://doi.org/10.1093/bioinformatics/btad028).

Correspondence and requests for materials should be addressed to rando@stanford.edu.

ACKNOWLEDGMENTS. We thank E. Brown for providing ATR^{fl/fl} mice. We thank B. Carter, C. Cain, and L. Rott and the Palo Alto VA Flow Cytometry Core for assistance with flow cytometry experiments. We thank R. Leib and K. Singhal and the Vincent Coates Foundation Mass Spectrometry Laboratory, Stanford University Mass Spectrometry core, for assistance with proteomics experiments. We thank H. Ishak, Y. Yu, and the entire T.A.R. lab for laboratory assistance and discussion. We thank the K.A.C. lab for additional expertise and discussion. This work was supported by funding from the Glenn Foundation for Medical Research, the Human Frontier Science Program (Award LT000028/2015-L to J.S.S.), the NIH (Grants P01 AG036695 and R01 AR073248 to T.A.R., and Grant R01 ES016486 to K.A.C.), and the Department of Veterans Affairs (BLR&D Merit Review Grant I01BX002324 to T.A.R.).

1. T. H. Cheung, T. A. Rando, Molecular regulation of stem cell quiescence. *Nat. Rev. Mol. Cell Biol.* **14**, 329–340 (2013).
2. C. T. J. van Velthoven, T. A. Rando, Stem cell quiescence: Dynamism, restraint, and cellular idling. *Cell Stem Cell* **24**, 213–225 (2019).

3. I. J. Cho *et al.*, Mechanisms, hallmarks, and implications of stem cell quiescence. *Stem Cell Reports* **12**, 1190–1200 (2019).
4. W. K. So, T. H. Cheung, Molecular regulation of cellular quiescence: A perspective from adult stem cells and its niches. *Methods Mol. Biol.* **1686**, 1–25 (2018).

5. Y. Liu *et al.*, p53 regulates hematopoietic stem cell quiescence. *Cell Stem Cell* **4**, 37–48 (2009).
6. R. A. Weinberg, The retinoblastoma protein and cell cycle control. *Cell* **81**, 323–330 (1995).
7. T. Cheng *et al.*, Hematopoietic stem cell quiescence maintained by p21^{cip1}/waf1. *Science* **287**, 1804–1808 (2000).
8. T. E. Kippin, D. J. Martens, D. van der Kooy, p21 loss compromises the relative quiescence of forebrain stem cell proliferation leading to exhaustion of their proliferation capacity. *Genes Dev.* **19**, 756–767 (2005).
9. T. Cheng, N. Rodrigues, D. Dombkowski, S. Stier, D. T. Scadden, Stem cell repopulation efficiency but not pool size is governed by p27(kip1). *Nat. Med.* **6**, 1235–1240 (2000).
10. C. R. Bjornson *et al.*, Notch signaling is necessary to maintain quiescence in adult muscle stem cells. *Stem Cells* **30**, 232–242 (2012).
11. S. Tümpel, K. L. Rudolph, Quiescence: Good and bad of stem cell aging. *Trends Cell Biol.* **29**, 672–685 (2019).
12. L. Liu *et al.*, Impaired notch signaling leads to a decrease in p53 activity and mitotic catastrophe in aged muscle stem cells. *Cell Stem Cell* **23**, 544–556.e4 (2018).
13. J. S. Cho, S. H. Kook, A. R. Robinson, L. J. Niedernhofer, B. C. Lee, Cell autonomous and nonautonomous mechanisms drive hematopoietic stem/progenitor cell loss in the absence of DNA repair. *Stem Cells* **31**, 511–525 (2013).
14. D. J. Rossi *et al.*, Deficiencies in DNA damage repair limit the function of haematopoietic stem cells with age. *Nature* **447**, 725–729 (2007).
15. D. J. Rossi *et al.*, Hematopoietic stem cell quiescence attenuates DNA damage response and permits DNA damage accumulation during aging. *Cell Cycle* **6**, 2371–2376 (2007).
16. L. Al Zouabi, A. J. Bardin, Stem cell DNA damage and genome mutation in the context of aging and cancer initiation. *Cold Spring Harb. Perspect. Biol.* **12**, a036210 (2020).
17. M. K. Zeman, K. A. Cimprich, Causes and consequences of replication stress. *Nat. Cell Biol.* **16**, 2–9 (2014).
18. F. A. Derheimer *et al.*, RPA and ATR link transcriptional stress to p53. *Proc. Natl. Acad. Sci. U.S.A.* **104**, 12778–12783 (2007).
19. E. Fanning, V. Klimovich, A. R. Nager, A dynamic model for replication protein A (RPA) function in DNA processing pathways. *Nucleic Acids Res.* **34**, 4126–4137 (2006).
20. L. Zou, S. J. Elledge, Sensing DNA damage through ATRIP recognition of RPA-ssDNA complexes. *Science* **300**, 1542–1548 (2003).
21. L. Kabeche, H. D. Nguyen, R. Buisson, L. Zou, A mitosis-specific and R loop-driven ATR pathway promotes faithful chromosome segregation. *Science* **359**, 108–114 (2018).
22. Y. Ruzankina, A. Asare, E. J. Brown, Replicative stress, stem cells and aging. *Mech. Ageing Dev.* **129**, 460–466 (2008).
23. Y. Ruzankina *et al.*, Deletion of the developmentally essential gene ATR in adult mice leads to age-related phenotypes and stem cell loss. *Cell Stem Cell* **1**, 113–126 (2007).
24. Y. Ruzankina *et al.*, Tissue regenerative delays and synthetic lethality in adult mice after combined deletion of Atr and Trp53. *Nat. Genet.* **41**, 1144–1149 (2009).
25. C. T. J. van Velthoven, A. de Morree, I. M. Egner, J. O. Brett, T. A. Rando, Transcriptional profiling of quiescent muscle stem cells in vivo. *Cell Rep.* **21**, 1994–2004 (2017).
26. L. Gay *et al.*, Mouse TU tagging: A chemical/genetic intersectional method for purifying cell type-specific nascent RNA. *Genes Dev.* **27**, 98–115 (2013).
27. J. C. Saldivar, D. Cortez, K. A. Cimprich, The essential kinase ATR: Ensuring faithful duplication of a challenging genome. *Nat. Rev. Mol. Cell Biol.* **18**, 622–636 (2017).
28. E. Olson, C. J. Nievera, V. Klimovich, E. Fanning, X. Wu, RPA2 is a direct downstream target for ATR to regulate the S-phase checkpoint. *J. Biol. Chem.* **281**, 39517–39533 (2006).
29. H. D. Nguyen *et al.*, Functions of replication protein A as a sensor of R loops and a regulator of RNaseH1. *Mol. Cell* **65**, 832–847.e4 (2017).
30. S. Hamperl, M. J. Bocek, J. C. Saldivar, T. Swigut, K. A. Cimprich, Transcription-replication conflict orientation modulates R-loop levels and activates distinct DNA damage responses. *Cell* **170**, 774–786.e19 (2017).
31. D. A. Matos *et al.*, ATR protects the genome against R loops through a MUS81-triggered feedback loop. *Mol. Cell* **77**, 514–527.e4 (2020).
32. L. Wahba, S. K. Gore, D. Koshland, The homologous recombination machinery modulates the formation of RNA-DNA hybrids and associated chromosome instability. *eLife* **2**, e00505 (2013).
33. P. Huertas, A. Aguilera, Cotranscriptionally formed DNA:RNA hybrids mediate transcription elongation impairment and transcription-associated recombination. *Mol. Cell* **12**, 711–721 (2003).
34. L. Wahba, J. D. Amon, D. Koshland, M. Vuica-Ross, RNase H and multiple RNA biogenesis factors cooperate to prevent RNA-DNA hybrids from generating genome instability. *Mol. Cell* **44**, 978–988 (2011).
35. A. De Magis *et al.*, DNA damage and genome instability by G-quadruplex ligands are mediated by R loops in human cancer cells. *Proc. Natl. Acad. Sci. U.S.A.* **116**, 816–825 (2019).
36. G. Miglietta, M. Russo, G. Capranico, G-quadruplex-R-loop interactions and the mechanism of anticancer G-quadruplex binders. *Nucleic Acids Res.* **48**, 11942–11957 (2020).
37. R. Rodriguez *et al.*, Small-molecule-induced DNA damage identifies alternative DNA structures in human genes. *Nat. Chem. Biol.* **8**, 301–310 (2012).
38. V. M. Vassin, R. W. Anantha, E. Sokolova, S. Kanner, J. A. Borowiec, Human RPA phosphorylation by ATR stimulates DNA synthesis and prevents ssDNA accumulation during DNA-replication stress. *J. Cell Sci.* **122**, 4070–4080 (2009).
39. V. M. Vassin, M. S. Wold, J. A. Borowiec, Replication protein A (RPA) phosphorylation prevents RPA association with replication centers. *Mol. Cell Biol.* **24**, 1930–1943 (2004).
40. E. J. Brown, D. Baltimore, Essential and dispensable roles of ATR in cell cycle arrest and genome maintenance. *Genes Dev.* **17**, 615–628 (2003).
41. P. Seale *et al.*, Pax7 is required for the specification of myogenic satellite cells. *Cell* **102**, 777–786 (2000).
42. I. M. Conboy, T. A. Rando, The regulation of Notch signaling controls satellite cell activation and cell fate determination in postnatal myogenesis. *Dev. Cell* **3**, 397–409 (2002).
43. M. Yamaguchi *et al.*, Calcitonin receptor signaling inhibits muscle stem cells from escaping the quiescent state and the niche. *Cell Rep.* **13**, 302–314 (2015).
44. A. de Morrée *et al.*, Staufen1 inhibits MyoD translation to actively maintain muscle stem cell quiescence. *Proc. Natl. Acad. Sci. U.S.A.* **114**, E8996–E9005 (2017).
45. H. Weintraub *et al.*, Muscle-specific transcriptional activation by MyoD. *Genes Dev.* **5**, 1377–1386 (1991).
46. F. A. Carrieri *et al.*, CDK1 and CDK2 regulate NICD1 turnover and the periodicity of the segmentation clock. *EMBO Rep.* **20**, e46436 (2019).
47. H. M. Shapiro, Flow cytometric estimation of DNA and RNA content in intact cells stained with Hoechst 33342 and pyronin Y. *Cytometry* **2**, 143–150 (1981).
48. M. Li *et al.*, MAP: Model-based analysis of proteomic data to detect proteins with significant abundance changes. *Cell Discov.* **5**, 40 (2019).
49. R. Choudhury *et al.*, The E3 ubiquitin ligase SCF(cyclin F) transmits AKT signaling to the cell-cycle machinery. *Cell Rep.* **20**, 3212–3222 (2017).
50. A. Lee *et al.*, Casein kinase II phosphorylation of cyclin F at serine 621 regulates the Lys48-ubiquitylation E3 ligase activity of the SCF^(cyclin F) complex. *Open Biol.* **7**, 170058 (2017).
51. I. Mavrommati *et al.*, β -TrCP- and casein kinase II-mediated degradation of cyclin F controls timely mitotic progression. *Cell Rep.* **24**, 3404–3412 (2018).
52. K. Burdova *et al.*, E2F1 proteolysis via SCF-cyclin F underlies synthetic lethality between cyclin F loss and Chk1 inhibition. *EMBO J.* **38**, e101443 (2019).
53. V. D'Angiolella, M. Esencay, M. Pagano, A cyclin without cyclin-dependent kinases: cyclin F controls genome stability through ubiquitin-mediated proteolysis. *Trends Cell Biol.* **23**, 135–140 (2013).
54. L. Clijsters *et al.*, cyclin F controls cell-cycle transcriptional outputs by directing the degradation of the three activator E2Fs. *Mol. Cell* **74**, 1264–1277.e7 (2019).
55. G. Yao, Modelling mammalian cellular quiescence. *Interface Focus* **4**, 20130074 (2014).
56. R. Choudhury *et al.*, APC/C and SCF(cyclin F) constitute a reciprocal feedback circuit controlling S-phase entry. *Cell Rep.* **16**, 3359–3372 (2016).
57. M. K. Tarrant *et al.*, Regulation of CK2 by phosphorylation and O-GlcNAcylation revealed by reanalysis. *Nat. Chem. Biol.* **8**, 262–269 (2012).
58. C. Borgo *et al.*, How can a traffic light properly work if it is always green? The paradox of CK2 signaling. *Crit. Rev. Biochem. Mol. Biol.* **56**, 321–359 (2021).
59. M. B. Baghdadi *et al.*, Reciprocal signalling by Notch-Collagen V-CALCR retains muscle stem cells in their niche. *Nature* **557**, 714–718 (2018).
60. T. H. Cheung *et al.*, Maintenance of muscle stem-cell quiescence by microRNA-489. *Nature* **482**, 524–528 (2012).
61. M. B. Baghdadi *et al.*, Notch-induced miR-708 antagonizes satellite cell migration and maintains quiescence. *Cell Stem Cell* **23**, 859–868.e5 (2018).
62. Y. A. Chan *et al.*, Genome-wide profiling of yeast DNA:RNA hybrid prone sites with DRIP-chip. *PLoS Genet.* **10**, e1004288 (2014).
63. C. T. Stork *et al.*, Co-transcriptional R-loops are the main cause of estrogen-induced DNA damage. *eLife* **5**, 5 (2016).
64. L. Wahba, L. Costantino, F. J. Tan, A. Zimmer, D. Koshland, S1-DRIP-seq identifies high expression and polyA tracts as major contributors to R-loop formation. *Genes Dev.* **30**, 1327–1338 (2016).
65. L. Chen *et al.*, R-ChIP using inactive RNase H reveals dynamic coupling of R-loops with transcriptional pausing at gene promoters. *Mol. Cell* **68**, 745–757.e5 (2017).
66. M. García-Rubio *et al.*, Yra1-bound RNA-DNA hybrids cause orientation-independent transcription-replication collisions and telomere instability. *Genes Dev.* **32**, 965–977 (2018).
67. C. Tous, A. Aguilera, Impairment of transcription elongation by R-loops in vitro. *Biochem. Biophys. Res. Commun.* **360**, 428–432 (2007).
68. T. García-Muse, A. Aguilera, R loops: From physiological to pathological roles. *Cell* **179**, 604–618 (2019).
69. A. Lockhart *et al.*, RNase H1 and H2 are differentially regulated to process RNA-DNA hybrids. *Cell Rep.* **29**, 2890–2900.e5 (2019).
70. K. A. Cimprich, D. Cortez, ATR: An essential regulator of genome integrity. *Nat. Rev. Mol. Cell Biol.* **9**, 616–627 (2008).
71. D. Hodroj *et al.*, An ATR-dependent function for the Ddx19 RNA helicase in nuclear R-loop metabolism. *EMBO J.* **36**, 1182–1198 (2017).
72. J. C. Saldivar *et al.*, An intrinsic S/G₂ checkpoint enforced by ATR. *Science* **361**, 806–810 (2018).
73. I. C. Wang *et al.*, Forkhead box M1 regulates the transcriptional network of genes essential for mitotic progression and genes encoding the SCF (Skp2-Cks1) ubiquitin ligase. *Mol. Cell Biol.* **25**, 10875–10894 (2005).
74. V. Petrovic, R. H. Costa, L. F. Lau, P. Raychaudhuri, A. L. Tyner, FoxM1 regulates growth factor-induced expression of kinase-interacting stathmin (KIS) to promote cell cycle progression. *J. Biol. Chem.* **283**, 453–460 (2008).
75. Y. Hou *et al.*, The transcription factor Foxm1 is essential for the quiescence and maintenance of hematopoietic stem cells. *Nat. Immunol.* **16**, 810–818 (2015).
76. E. J. Brown, D. Baltimore, ATR disruption leads to chromosomal fragmentation and early embryonic lethality. *Genes Dev.* **14**, 397–402 (2000).
77. A. de Klein *et al.*, Targeted disruption of the cell-cycle checkpoint gene ATR leads to early embryonic lethality in mice. *Curr. Biol.* **10**, 479–482 (2000).
78. Y. Lee *et al.*, ATR maintains select progenitors during nervous system development. *EMBO J.* **31**, 1177–1189 (2012).
79. A. Poppy Roworth, F. Ghari, N. B. La Thangue, To live or let die – Complexity within the E2F1 pathway. *Mol. Cell Oncol.* **2**, e970480 (2015).
80. A. C. Phillips, S. Bates, K. M. Ryan, K. Helin, K. H. Vousden, Induction of DNA synthesis and apoptosis are separable functions of E2F-1. *Genes Dev.* **11**, 1853–1863 (1997).
81. N. Pediconi *et al.*, Differential regulation of E2F1 apoptotic target genes in response to DNA damage. *Nat. Cell Biol.* **5**, 552–558 (2003).
82. L. Liu, T. H. Cheung, G. W. Charville, T. A. Rando, Isolation of skeletal muscle stem cells by fluorescence-activated cell sorting. *Nat. Protoc.* **10**, 1612–1624 (2015).